Performance analysis of a stand-alone synchronous reluctance generator under unbalanced conditions

Mostafa Rida[1], Essam Rashad[2], Adel El Samahy[1], Mohamed El Koroflly[1], Erhab Youssef[1]
[1]Department of Electrical Power and Machines, Faculty of Engineering, Helwan University (FEHU), Cairo, Egypt
[2]Department of Electrical Power and Machines, Faculty of Engineering, Tanta University (FETU), Tanta, Egypt

Article Info

ABSTRACT

A stand-alone self-excited wind energy conversion system (WECS) is considered commonly used in remote areas due to its simple control and low cost. This paper introduces the performance analysis of a stand-alone self-excited reluctance generator (SERG) under balanced and unbalanced operations. An asymmetrical component is proposed to obtain the positive and negative sequence components of voltages and currents in addition to the unbalanced voltage factor of SERG. The obtained results have been validated and compared with experimental results obtained from a laboratory prototype of a 5.5 kW synchronous reluctance generator driven by a dc motor as a prime-mover under unbalanced excitation capacitors and unbalanced loads. The comparison verifies the applicability of the proposed model.

Corresponding Author:

Mostafa Rida
Department of Electrical Power and Machines, Faculty of Engineering, Helwan University
1 Sherif St, Helwan, P.O 11792, Helwan, Cairo, Egypt
Email: Mostafarida@h-eng.helwan.edu.eg

1. INTRODUCTION

Due to increasing energy demand and climate changes, renewable energy sources (RES) have become a crucial energy transformation to reduce carbon emissions. In recent years, RES have been getting worldwide strong attention. In particular, hydropower, geothermal power, solar energy, and wind energy [1]. According to international renewable energy agency (IRENA), wind energy is the most significant growing uninterrupted worldwide a rate of attractive much 7.5 giga watt (GW) in the past twenty years, that brisk from 7.5 GW in 1997 to 700 GW by 2020. Therefore, the wind energy source has become prominent for both isolated and grid-connected systems [2]. Doubly fed induction generator (DFIG) and permanent magnet synchronous generator (PMSG) are the choice of the most proper generator for wind energy conversion systems (WECS). However, the utilization of rare earth magnets in PMSG is the major limitation due to demagnetization at a higher temperature and cogging torque effects. In addition, the cost of PMSG, which has endured a rise in varieties in the last years, leads researchers to search for new alternatives [2]–[5].

Regarding DFIG, its construction makes it an attractive selection for integrating WECS into the grid [6] due to the dual output ability of DFIG through both the stator and the rotor. As a result, the sizing of the power converter reduces, and it is 30% of its stator rating and harmonics filter as well. Furthermore, there is no need for an external reactive power source because the required excitation for DFIG is supplied from the rotor circuit through the power converter. However, the presence of slip rings and brushes results in regular maintenance, which leads the use of DFIG in off-shore applications less dependable and costly. Besides, the large size makes it not suitable for small stand-alone applications [7], [8].

Consequently, a stand-alone self-excited WECS is a popular candidate in remote areas; the self-excited induction generator (SEIG) is commonly used in stand-alone WECS [9]. Owing to many advantages such as no brushes, less maintenance, less cost, and the capability to control power at variable speeds [10]. On the other hand, the regular brushless self-excited generators' performance is poor in terms of voltage regulation, which requires a magnetizing current from an external excitation source such as additional excitation capacitances. Additionally, the output voltage and frequency of SEIG are significantly affected by the variation of speed and load. These drawbacks have been introduced and studied to enhance the power quality that increases the installation cost [10]–[13].

Currently, synchronous reluctance generator (SRG) has been developed to become an alternative for PMSG and DFIG because it has promising features such as high efficiency, small size, no need for permanent magnets, and free maintenance due to the absence of brushes [14], [15]. Moreover, it has the same advantages as SEIG and other features, such as less core loss, less noise, and rotor copper lossless. Then, at that point, SRG exhibits characteristics highly attractive for stand-alone WECS applications [2], [5], [10], [14]. Also, when derived at a constant, SRG provides a constant output frequency for variable loads and excitation capacitances and improves the steady-state performance over a wide range of operations. Tremendous efforts have been devoted to studying the performance of an isolated self-excited reluctance generator (SERG) at steady-state and dynamic operations. In [2], [10]–[14], [16]–[18], the authors have studied a linearized model of SERG to obtain the eigenvalues of speed, excitation capacitance, and load for steady-state stability under a wide range of different operating conditions. All articles have investigated the SERG performance in steady-state operation; until now, the SERG performance under abnormal conditions such as unbalanced loads or unbalanced excitation capacitors has not been widely researched [19].

During unbalanced operations, the unbalanced terminal voltage and stator currents of SERG are generated, introducing positive, negative, and zero sequence components. The positive sequence component produces a rotating magnetomotive force (MMF) in the air gap, rotating at synchronous speed. In contrast, MMF rotates in the opposite direction at synchronous speed for the negative sequence component, resulting in oscillations with double frequency. Regarding the zero-sequence component, it is canceled out, and no MMF in the machine air gap; because of the 120° electric displacement angle between the three-phase stator windings, which have the same angular displacement all time [20], [21]. The unbalanced stator currents produce a ripple torque that causes mechanical stress on the rotor shaft, in addition to the temperature rise of the stator, which degrades the stator winding insulation [22]–[24]. Nevertheless, researchers have simulated and validated SERG experimentally using a modified squirrel cage induction machine or salient pole synchronous machine, not from the machine of flux barriers rotor.

This paper concentrates on the performance analysis of a stand-alone SERG under unbalanced conditions at unbalanced excitation capacitance and unbalanced loads. Analysis symmetrical components have been adopted to obtain the factor of unbalanced voltage, currents, power, and torque of SERG under unbalanced conditions. The calculated results are validated using experimental results obtained from laboratory SRG of a rotor with flux barriers. This paper is organized into three sections. The modeling of the stand-alone SERG system, the computational procedure of the excitation capacitance, and performance analysis under unbalanced conditions are derived and demonstrated in section 2. Then, the simulation and experimental results for the performance of the proposed system under balanced and unbalanced operations are presented and investigated in section 3. Finally, the conclusion is presented in section 4.

2.   PROPOSED SERG STAND-ALONE SYSTEM

This paper proposes and analyses a synchronous reluctance generator with no damper winding and flux barriers rotor. SERG is connected to a three-phase load and excitation capacitances to operate in a stand-alone system. The schematic diagram and experimental setup of proposed system are shown in Figure 1.

2.1. SERG mathematical model

Dynamic modeling equations of SERG are derived using Park's d-q axes transformation. The machine reluctance can be obtained from those of the wound field synchronous machine with the field winding terms omitted [2], [5]. To simplify the dynamic modeling of SERG, the following assumptions are considered [2], [10], [16].
−   The core losses of the machine are neglected
−   The effect of saturation is considerable in d-axis only
−   Neglect harmonics in the MMF and air-gap flux

The steady-state model equations of SERG are obtained by considering the rate change of flux linkage rate is zero. Hence, the steady-state model of SERG in the d-q rotor reference frame is expressed using (1) and (2) listed by [2], [10], [16].

$$V_{qs} = -r_s i_q - \omega_r \lambda_{ds} = -r_s i_q + \frac{\omega_r}{\omega_b} X_d i_d \tag{1}$$

$$V_{ds} = -r_s i_d + \omega_r \lambda_{qs} = -r_s i_d - \frac{\omega_r}{\omega_b} X_q i_q \tag{2}$$

Where (V_{qs}, V_{ds}) are the stator voltages in the q-d axes frame, (i_q, i_d) are stator currents in d-q axes, $(\lambda_{qs}, \lambda_{ds})$ are the stator linkage flux in q-d axes, r_s represents the stator resistance, (X_d, X_q) are the stator direct and quadrature axis reactance respectively at base frequency, whiles (ω_b, ω_r) are the synchronous and rotor speeds in rad/s, respectively.

(a)   (b)
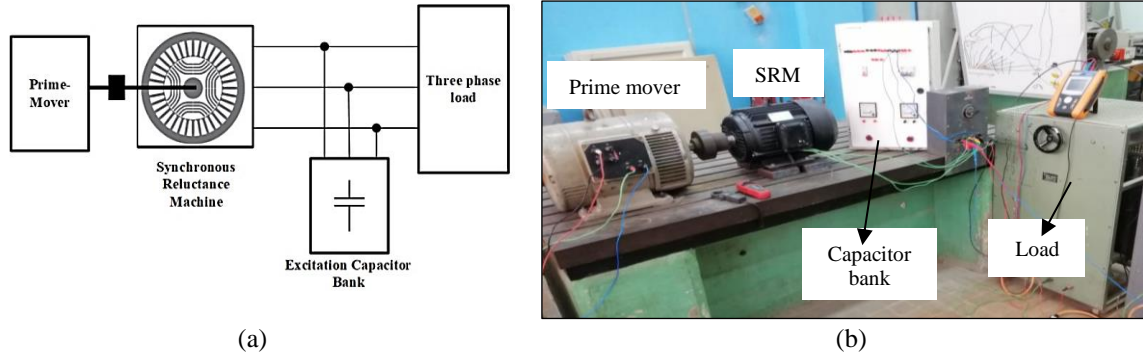
Figure 1. Representation of the proposed system: (a) schematic diagram and (b) experimental setup

The flux linkages in d-q axis coordinators can be obtained by (3) and (4), where L_d and L_q are the stator inductors in the direct and quadrature axis, respectively.

$$\lambda_q = -L_q i_q \tag{3}$$

$$\lambda_d = -L_d i_d \tag{4}$$

Regarding the generator electromagnetic torque developed, T_e is obtained by (5). T_e is expressed as a function of inductance in (6) by substituting (3) and (4) in (5), where $k = \frac{3}{4}p$, and p is the number of poles of the SERG.

$$T_e = k(\lambda_d I_q - \lambda_q I_d) \tag{5}$$

$$T_e = k(L_d - L_q)I_d I_q \tag{6}$$

Figure 2(a) and Figure 2(b) represent the steady-state equivalent circuit of SERG in d-q axis, respectively, with excitation capacitor (C) and loads (R_L, X_L, Z_L). Figure 3 illustrates the phasor diagram of the equivalent circuit of SERG. Refereeing to the phasor diagram of SERG in Figure 3, the equations of stator voltage and currents in the d-q axis frame can be determined as described in (7)-(10), where I_c, I_L are the capacitance and load currents respectively, δ represents the load angle, $\emptyset$ is the power angle and $V_t = X_c I_c = Z_L I_L$.

$$V_{ds} = -V_t \sin\delta = -X_c I_c \sin\delta \tag{7}$$

$$V_{qs} = -V_t \cos\delta = X_c I_c \cos\delta \tag{8}$$

$$I_d = -I_L \sin(\delta + \emptyset) + I_c \cos\delta \tag{9}$$

$$I_q = I_L \cos(\delta + \emptyset) + I_c \sin\delta \tag{10}$$
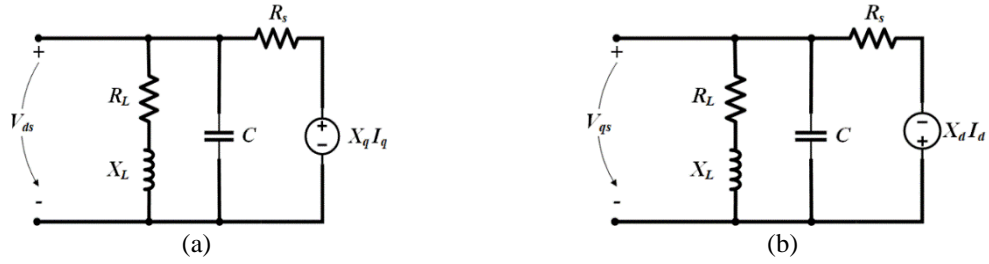
Figure 2. The equivalent circuit of SERG in steady-state, (a) d-axis, and (b) q-axis
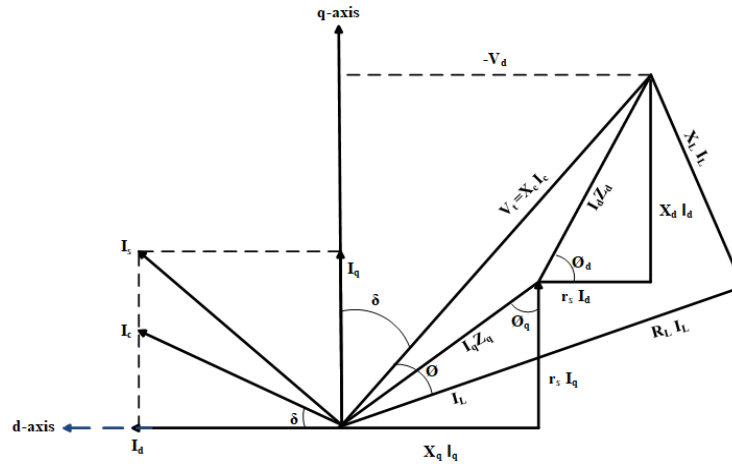

Figure 3. Steady-state SERG phasor diagram

To obtain the terminal voltage V_t, the load angle δ and X_d will be calculated. In [2], the mathematical procedures to obtain these parameters are discussed in detail. Hence, V_t is given by (11).

$$V_t = I_d \frac{Z_L * X_c}{Z_L * \cos\delta - X_c * \sin\delta} \tag{11}$$

Where I_d is calculated as a function of X_d using (12). It is obtained experimentally at the base frequency based on the magnetization curve of a 5.5 kW SRG. Curve fitting is used to model a 4th-order polynomial function.

$$I_d = 3.723 * 10^{-8}X_d{}^4 - 0.001271X_d{}^3 + 0.1534X_d{}^2 - 6.393X_d + 97.03 \tag{12}$$

The excitation capacitor value necessary to operate the SERG at any load conditions or speed profile is calculated using the steady-state in (2) to (8).

2.2. The SERG analysis under abnormal conditions

Normally, SERG operates appropriately in a balanced operation under balanced excitation capacitors and loads. However, the unbalanced conditions could occur by loads or excitation capacitances, so the effects of unbalancing conditions on the generator's terminal voltage and currents are investigated by obtaining the positive, negative, and zero components. According to that, the produced voltage can be obtained using (13) and (15) by assuming the load/or the excitation capacitor of both phases (b) and (c) are kept the same resistance value, and the load/or the excitation capacitor connected to phase (a) is varied.

$$\begin{bmatrix} V_a \\ V_b \\ V_c \end{bmatrix} = V_s{}^+ \begin{bmatrix} \cos(\omega t + \Phi^+) \\ \cos(\omega t + \Phi^+ - 120°) \\ \cos(\omega t + \Phi^+ + 120°) \end{bmatrix} + V_s{}^- \begin{bmatrix} \cos(-\omega t + \Phi^-) \\ \cos(-\omega t + \Phi^- - 120°) \\ \cos(-\omega t + \Phi^- + 120°) \end{bmatrix} + V_s{}^0 \begin{bmatrix} \cos(\omega t + \Phi^0) \\ \cos(\omega t + \Phi^0) \\ \cos(\omega t + \Phi^0) \end{bmatrix} \tag{13}$$

Where $(V_s{}^+ . V_s{}^- . V_s{}^0)$ are the amplitude voltage of the positive, negative and zero sequence components respectively, ω is the angular frequency of fundamental voltage, and $(\Phi^+ . \Phi^- . \Phi^0)$ represents the phase angles of voltage sequence components as described in [20], [25]–[27].

Applying Concordia transformation (14) to (13), the variables X_{abc} are hence transformed to $\alpha\beta\gamma$ coordinates, where $X_{\alpha\beta\gamma} = C^T X_{abc}$, whereas the component of zero-sequence has no effect on the performance of SERG. Thus, the voltage can be represented in $\alpha\beta$ frame and obtained from (15).

$$C = \begin{bmatrix} 1 & -0.5 & -0.5 \\ 0 & 0.866 & -0.866 \\ 0.5 & 0.5 & 0.5 \end{bmatrix} \tag{14}$$

$$V_{s(\alpha\beta)} = \begin{bmatrix} V_\alpha \\ V_\beta \end{bmatrix} = V_{s(\alpha\beta)}{}^+ + V_{s(\alpha\beta)}{}^- = V_s{}^+ \begin{bmatrix} \cos(\omega t + \Phi^+) \\ \sin(\omega t + \Phi^+) \end{bmatrix} + V_s{}^- \begin{bmatrix} \cos(-\omega t + \Phi^-) \\ \sin(-\omega t + \Phi^-) \end{bmatrix} \tag{15}$$

Then, $V_{s(dq)}$ can be further obtained using Park transformation from $X_{dq} = D_{dq} X_{\alpha\beta}$. Whereas D_{dq} represents the matrix transformation $(D_{(dq)}{}^+ . D_{(dq)}{}^-)$, and calculated using the following equations, where θ is the rotation angle of the reference d-q frame.

$$D_{(dq)}{}^+ = \begin{bmatrix} \cos\theta & \sin\theta \\ -\sin\theta & \cos\theta \end{bmatrix}, \text{ and } D_{(dq)}{}^- = \begin{bmatrix} \cos\theta & -\sin\theta \\ \sin\theta & \cos\theta \end{bmatrix} \tag{16}$$

By applying Park transformation (16) to (15), the terminal voltage V_s in d-q frame can be expressed as:

$$V_{s(dq)}{}^- = \begin{bmatrix} V_{s(d)}{}^- \\ V_{s(q)}{}^- \end{bmatrix} = D_{(dq)}{}^- \begin{bmatrix} V_\alpha \\ V_\beta \end{bmatrix} = V_s{}^+ \begin{bmatrix} \cos(\omega t + \Phi^+ + \theta) \\ \sin(\omega t + \Phi^+ + \theta) \end{bmatrix} + V_s{}^- \begin{bmatrix} \cos(-\omega t + \Phi^- + \theta) \\ \sin(-\omega t + \Phi^- + \theta) \end{bmatrix} \tag{17}$$

$$V_{s(dq)}{}^+ = \begin{bmatrix} V_{s(d)}{}^+ \\ V_{s(q)}{}^+ \end{bmatrix} = D_{(dq)}{}^+ \begin{bmatrix} V_\alpha \\ V_\beta \end{bmatrix} = V_s{}^+ \begin{bmatrix} \cos(\omega t + \Phi^+ - \theta) \\ \sin(\omega t + \Phi^+ - \theta) \end{bmatrix} + V_s{}^- \begin{bmatrix} \cos(-\omega t + \Phi^- - \theta) \\ \sin(-\omega t + \Phi^- - \theta) \end{bmatrix} \tag{18}$$

The phase lock is achieved by setting the phase angle $\theta = \omega t$. Thus, the positive terminal voltages V_s can be expressed in d-q frame by (19).

$$\begin{bmatrix} V_{s(d)}{}^+ \\ V_{s(q)}{}^+ \end{bmatrix} = V_s{}^+ \begin{bmatrix} \cos(\Phi^+) \\ \sin(\Phi^+) \end{bmatrix} + V_s{}^- \cos(\Phi^-) \begin{bmatrix} \cos(2\omega t) \\ -\sin(2\omega t) \end{bmatrix} + V_s{}^- \sin(\Phi^-) \begin{bmatrix} \sin(2\omega t) \\ \cos(2\omega t) \end{bmatrix} \tag{19}$$

And the negative terminal voltage in d-q frame by (20).

$$\begin{bmatrix} V_{s(d)}{}^- \\ V_{s(q)}{}^- \end{bmatrix} = V_s{}^- \begin{bmatrix} \cos(\Phi^-) \\ \sin(\Phi^-) \end{bmatrix} + V_s{}^+ \cos(\Phi^+) \begin{bmatrix} \cos(2\omega t) \\ \sin(2\omega t) \end{bmatrix} + V_s{}^+ \sin(\Phi^+) \begin{bmatrix} -\sin(2\omega t) \\ \cos(2\omega t) \end{bmatrix} \tag{20}$$

From (19) and (20), it can be observed that the DC component is the positive-sequence component of the positive component $V_{s(dq)}$ and the AC component with frequency 2ω is the negative-sequence component of $V_{s(dq)}{}^+$ in contrast to the negative component of $V_{s(dq)}{}^-$. The AC component with frequency 2ω is the positive-sequence component, and the DC component is the negative-sequence component.

Accordingly, the positive and negative sequence components of current can be obtained by (21).

$$\begin{bmatrix} I_{(d)}{}^+ \\ I_{(q)}{}^+ \end{bmatrix} = I_s{}^+ \begin{bmatrix} \cos(\Phi_i{}^+) \\ \sin(\Phi_i{}^+) \end{bmatrix} + I_s{}^- \cos(\Phi_i{}^-) \begin{bmatrix} \cos(2\omega t) \\ -\sin(2\omega t) \end{bmatrix} + I_s{}^- \sin(\Phi_i{}^-) \begin{bmatrix} \sin(2\omega t) \\ \cos(2\omega t) \end{bmatrix} \tag{21}$$

And the negative current in d-q frame by (22).

$$\begin{bmatrix} I_{(d)}{}^- \\ I_{(q)}{}^- \end{bmatrix} = I_s{}^- \begin{bmatrix} \cos(\Phi_i{}^-) \\ \sin(\Phi_i{}^-) \end{bmatrix} + I_s{}^+ \cos(\Phi_i{}^+) \begin{bmatrix} \cos(2\omega t) \\ \sin(2\omega t) \end{bmatrix} + I_s{}^+ \sin(\Phi_i{}^+) \begin{bmatrix} -\sin(2\omega t) \\ \cos(2\omega t) \end{bmatrix} \tag{22}$$

Regarding the real and reactive powers developed by the generator for a balanced system, these are given by (23) [28].

$$\begin{cases} P_g = k(V_{sd} i_d + V_{sq} i_q) \\ Q_g = k (V_{sd} i_q - V_{sq} i_d) \end{cases} \tag{23}$$

Consequently, for unbalanced operation, the P_g and Q_g can be obtained from the voltages and currents' positive and negative sequence components. Thus, the active and reactive power can be expressed as (24).

$$\begin{cases} P_g = P_{gdc} + P_{gcos} \cos(2wt) + P_{gsin} \sin(2\omega t) \\ Q_g = Q_{gdc} + Q_{gcos} \cos(2wt) + Q_{gsin} \sin(2\omega t) \end{cases} \tag{24}$$

where (P_{gdc}, Q_{gdc}) represent the average values of the generator instantaneous active and reactive power respectively, and $(P_{gcos}, P_{gsin}, Q_{gcos}, Q_{gsin})$ are the second-order oscillations in terms of the instantaneous powers.

Thus, the active power for unbalanced operation is given by (25).

$$\begin{cases} P_{gdc} = k \left(V_{sd}{}^+ I_d{}^+ + V_{sq}{}^+ I_q{}^+ + V_{sd}{}^- I_d{}^- + V_{sq}{}^- I_q{}^- \right) \\ P_{gcos} = k \left(V_{sd}{}^- I_d{}^+ + V_{sq}{}^- I_q{}^+ + V_{sd}{}^+ I_d{}^- + V_{sq}{}^+ I_q{}^- \right) \\ P_{gsin} = k \left(V_{sq}{}^- I_d{}^+ - V_{sd}{}^- I_q{}^+ - V_{sq}{}^+ I_d{}^- + V_{sd}{}^+ I_q{}^- \right) \end{cases} \tag{25}$$

And the reactive power for unbalanced operation is given by (26).

$$\begin{cases} Q_{gdc} = k \left(V_{sq}{}^+ I_d{}^+ - V_{sd}{}^+ I_q{}^+ + V_{sq}{}^- I_d{}^- + V_{sd}{}^- I_q{}^- \right) \\ Q_{gcos} = k \left(V_{sq}{}^- I_d{}^+ - V_{sd}{}^- I_q{}^+ + V_{sq}{}^+ I_d{}^- - V_{sd}{}^+ I_q{}^- \right) \\ Q_{gsin} = k \left(-V_{sd}{}^- I_d{}^+ - V_{sq}{}^- I_q{}^+ + V_{sd}{}^+ I_d{}^- + V_{sq}{}^+ I_q{}^- \right) \end{cases} \tag{26}$$

As a result, the electric torque of the SERG T_g can be expressed as a function of active power as (27).

$$T_g = \frac{P_g}{\omega_r} = T_{gdc} + T_{gcos} \cos(2\omega t) + T_{gsin} \sin(2\omega t) \tag{27}$$

The second-order oscillations terms of the electric torque are given by (28), and $T_{gcos} = 0$.

$$\begin{cases} T_{gdc} = k \left(L_d - L_q \right) \left[I_q{}^+ I_d{}^+ + I_q{}^- I_d{}^- \right] \\ T_{gsin} = k \left(L_d - L_q \right) \left[I_q{}^- I_d{}^+ + I_q{}^+ I_d{}^- \right] \\ T_{gcos} = k \left[-L_d I_d{}^- I_d{}^+ - L_q I_q{}^- I_q{}^+ + L_d I_d{}^- I_d{}^+ + L_q I_q{}^- I_q{}^+ \right] \end{cases} \tag{28}$$

2.3. Unbalanced voltage definitions

The unbalanced voltage can be measured using three definitions based on standards [21], [27] as described below:

− The phase voltage unbalance rate (PVUR) definition is given by IEEE Std 141 and obtained by (29), where the SERG phase voltages (V_a. V_b. V_c) are used for calculation.

$$PVUR = \frac{\max(|V_a| - |V_{mean}|, |V_b| - |V_{mean}|, |V_c| - |V_{mean}|)}{V_{mean}} * 100 \tag{29}$$

− The line voltage unbalance rate (LVUR) definition is introduced by the National Electrical Manufacturers Association (NEMA). Whereas the maximum voltage variation from the average line voltage magnitude to the average line voltage magnitude is calculated as a percentage of the average line voltage magnitude as (30).

$$LVUR = \frac{\max(|V_{ab}| - |V_{mean}|, |V_{bc}| - |V_{mean}|, |V_{ca}| - |V_{mean}|)}{V_{mean}} * 100 \tag{30}$$

− The voltage unbalanced factor (VUF) is defined by the international electrotechnical commission (IEC) as follows, where $(V_s{}^+, V_s{}^-)$ are the voltage amplitude of the positive sequence and negative sequence component of the SERG terminal voltages.

$$VUF = \frac{V_s{}^-}{V_s{}^+} * 100 \tag{31}$$

3.   RESULTS AND DISCUSSION

This section presents the validation of SRG with cageless and flux barriers rotor rated (340 V, 5.5 kW, 50 Hz, four poles) as listed in Table 1. It is modeled using MATLAB/Simulink environment and the experimental set-up in the laboratory. The obtained results are validated and studied under balanced and unbalanced operations. The machine parameters of SRG are predetermined using simple standard off-line tests such as DC, locked rotor, and no-load tests discussed in [11], [22]; after that, the analytical performance of SRG magnetizing characteristics (I_d-X_d) is obtained by the no-load test as shown in Figure 4.

Table 1. Machine parameters at 50 Hz

Machine rating (kW)	Terminal voltage (V)	R_s (Ω)	Unsaturated L_d (H)	Unsaturated L_q (H)	Rated speed (r.p.m)
5.5	340	0.6	0.1331	0.05195	1500
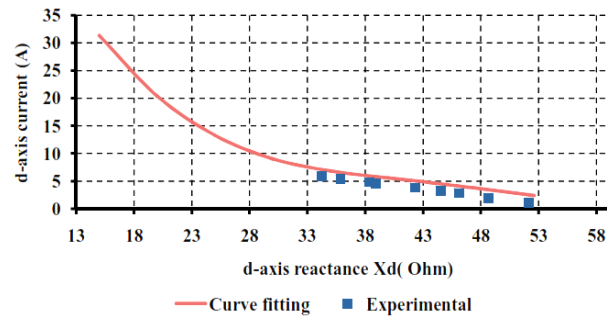
Figure 4. The magnetizing characteristics of the SERG machine at the base frequency

3.1. Balanced operation

In this case, SERG driven by a variable speed dc motor is studied under variable load impedance, generator speed and load power factor. The SERG operates with symmetrical excitation capacitance and symmetrical load impedance. Figure 5 and Figure 6 show the calculated and experimental results of the load characteristics (V-I) of SERG at unity power factor, speed 1450 rpm and excitation capacitance = 100 μF. It is observed that the terminal voltage and the excitation capacitance current decrease at the load current increases, as listed in Table 2 as well.

The proposed system is tested at different values of the excitation capacitance, as listed in Table 3, and it can be observed that the capacitance is varied inversely with the SERG speed. Experimental and calculated results are depicted in Figure 7. Figure 8 and Figure 9 show the terminal voltage characteristics with load current variation under various load impedance at different values of excitation capacitance and generator speed (Nr) is 1500 rpm. It can be noticed that the terminal voltage falls as the load current increases with lagging power decreases. The output power increases when the load current increases for higher speeds and slightly decreases with load current increases at each speed as shown in Figure 10.
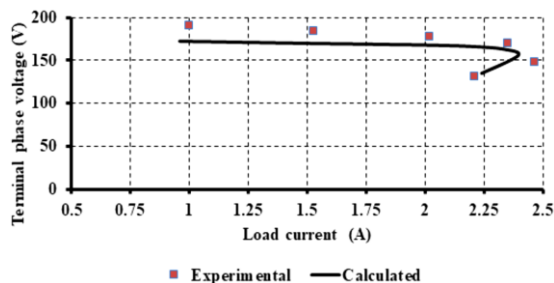

Figure 5. Terminal voltage variation against load current at unity power factor at constant capacitance and constant speed
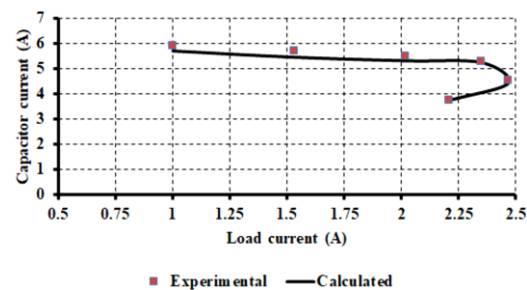

Figure 6. Capacitor current variation against load current variation at constant capacitance and constant speed

Table 2. Experimental results for steady-state operation at unity power factor, C=100 µf and speed
1450 r.p.m

Load current (A)	Terminal voltage(V)	Capacitor current (A)
2.2111	131.5	3.75
2.467	147.8	4.52
2.35	169.85	5.3
2.02	176.957	5.5
1.53	183.6	5.71
1	190.525	5.9

Table 3. Experimental results of the excitation capacitance variation with the generator speed

Generator speed (r.p.m.)	1818	1668	1550	1481	1397	1372	1274
Excitation capacitance (µf)	51.5	60	70	80	91.5	100	131.5
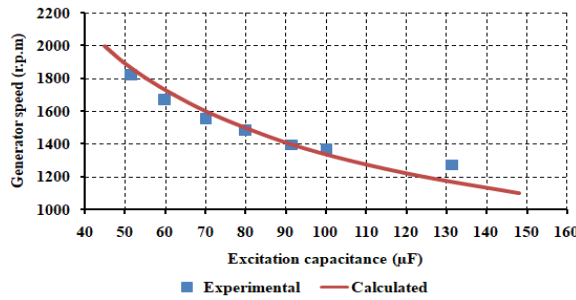
Figure 7. Excitation capacitance with the generator speed variation at no load at rated voltage
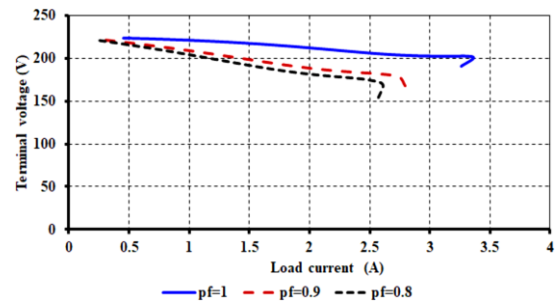
Figure 8. Terminal voltage variation against load current at different power factor, C=120µF and constant speed
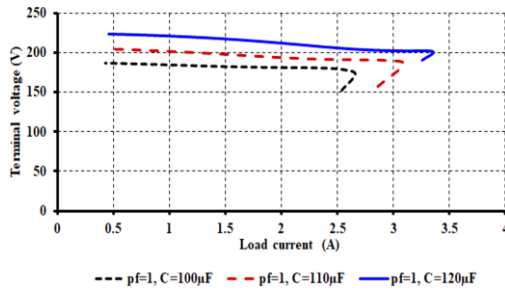
Figure 9. Terminal voltage variation against load current at different excitation capacitance and constant speed
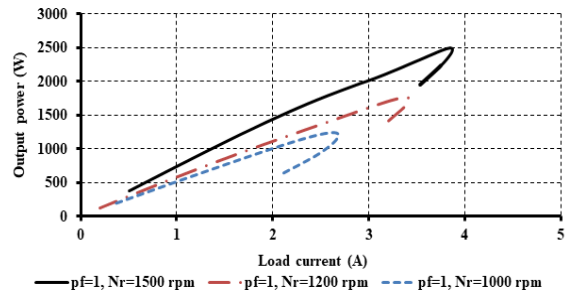
Figure 10. Output power variation against load current at a different speed, and constant excitation capacitance

3.2. Unbalanced operation

This case presents the experimental and calculated results of SERG under unbalanced operation studied at unsymmetrical load and unsymmetrical excitation capacitance. Symmetrical components are used to calculate the positive and negative sequence components for voltages and currents that are generated during unbalance operation. In addition, the voltage unbalanced factor VUF is calculated as well.

3.2.1. Case study I

The terminals of generator SRG are connected to unsymmetrical capacitances in this case. This means the phase terminal (b) is connected to varying capacitances different from the capacitance connected at the other terminals of phases (a) and (c). Consider the excitation capacitance base value is C=161.5 µF at normal operation to ensure the terminal phase voltage $V_{T=}$164 V at resistive load base value R_L=113.8 Ω and Nr=1200 rpm. Hence, the experimental results are obtained at a constant value of capacitance connected for phases (a) and (c) at C=1 pu while the capacitance connected to phase (b) varies from 1 pu to 1.3715 pu of base capacitance value as tabulated in Table 4. Figure 11 shows the percentage value of UVF is varied by varying

the capacitance connected to phase (b) below 0.8pu to above 1.3715 pu with keeping the capacitance connected to other constant. It can be seen that the zero value of UVF is the balanced point when the connected excitation capacitance for phase (b) is 1 pu or symmetrical excitation capacitance.

      Figure12 shows the variation of positive and negative sequence components of voltages against the unbalance voltage factor UVF, whereas the negative-sequence voltage varies experimentally from 0% to 24.94% and the positive-sequence voltage from 100% to 97.43%at capacitor changes from $C=1$ pu to $C=1.3715$ pu. Regarding the calculated results, the negative-sequence voltage varies from -27.92% to 32.9% and the positive-sequence voltage varies from 96.96% to 103.24% at $C=0.8$ pu and increases to 1.3715 pu. The positive sequence voltage varies from 94.65% to 97.4% of the operating phase voltage. Figure13 shows the effect of negative-sequence voltage on the negative sequence current produced by SERG. The resulting negative sequence currents vary with the degree of unbalanced voltage factor almost linearly varied from 0 to 25.4% experimentally and from -25.41% to 33.4% calculated.

Table 4. Experimental results at unsymmetrical excitation capacitance

| Excitation capacitance connected to Phase (b)	1 pu	1.062 pu	1.124 pu	1.186 pu	1.2476 pu	1.372 pu
V_a	162.9	165.3	166.9	169.5	168	171.2
V_b	164.1	163.4	163.9	164.8	163	165
V_c	163.8	164.6	166	166	165.4	165.8
V_p	163.59	164.12	164.58	164.68	161.97	159.8
V_n	0.248	7.425	13.46	20.356	26.02	39.86
UVF%	0.152	4.524	8.179	12.361	16.07	24.94
I_a	7	7	7.4	7.5	7.8	7.9
I_b	7.1	7.1	7.1	7.3	7.2	7.2
I_c	6.8	6.9	6.9	6.9	7	7
I_p	6.9666	6.991	7.096	7.152	7.195	7.11
I_n	0.094	0.274	0.666	0.95	1.281	1.73
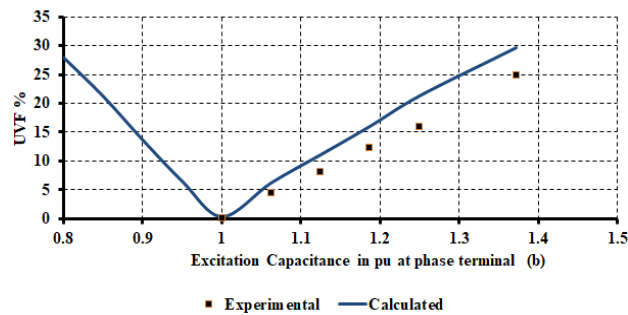
Figure 11. The UVF variation against unsymmetrical capacitance in pu
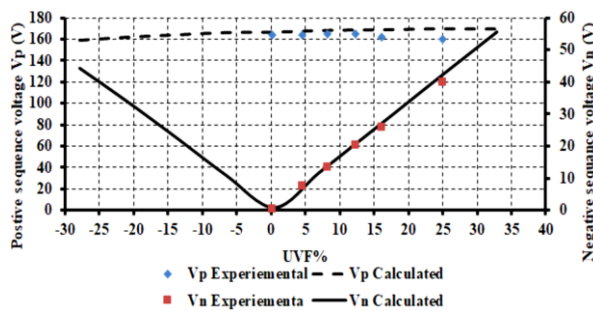
Figure 12. Variation of positive and negative sequence components of phase voltage against UVF
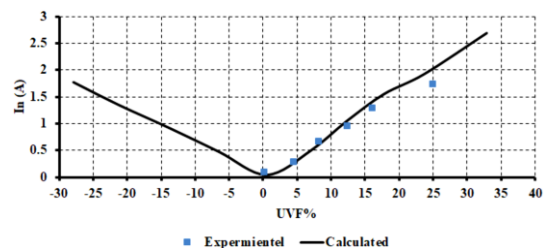
Figure 13. Variation of the negative current sequence component against UVF

3.2.2. Case study II

      This case studies the performance of SERG under unsymmetrical loads. By connecting the phase terminal (b) of the generator to various load impedance with keeping the load impedance of the other phases terminals (a) and (c) constant. For normal operation, the obtained results are validated at C=161.5 μF,

Vt=170 V and Nr=1216 rpm. The experimental results tabulated in Table 5 are collected by varying the load resistance connected to phase (b) from 1pu to 1.673pu and open phase case.

Table 5. Experimental results at unsymmetrical load impedance

Load at Phase (b)	1 pu	1.065 pu	1.097 pu	1.1617 pu	1.2162 pu	1.397 pu	1.673 pu	open phase
V_a	169.2	169.2	170.3	171.3	170.6	172.8	174.2	187.7
V_b	170	170	171	172	171.2	173.9	175.5	190.8
V_c	169.7	169.8	170.6	171.2	170.2	171.7	174.2	178.8
V_p	169.632	169.653	170.606	171.434	170.553	172.431	173.74	176.2
V_n	0.269	1.530	2.228	3.580	4.697	8.64	12.911	45.63
UVF%	0.159	0.902	1.306	2.088	2.754	5.0102	7.431	25.9
I_a	7.3	7.4	7.2	7.2	7.1	7.5	7.4	8.3
Ib	7.4	7.6	7.3	7.5	7.4	7.8	7.7	9.4
I_c	7.2	7.3	7.2	7.1	7	7.1	7.4	7.2
I_p	7.3	7.433	7.232	7.2631	7.161	7.453	7.473	7.98
I_n	0.07	0.153	0.1355	0.280	0.322	0.517	0.554	2.32

The calculated and experimental results of UVF are obtained at the resistive load connected to phase (b) varies from 0.5 pu to 1.673 pu and keeps the load at other phases constant, as shown in Figure 14. Whereas the zero value of UVF is considered the balanced point at the connected load for phase (b) is 1 pu, or the three-phase voltages are equal at symmetrical three-phase load.

Figure 15 shows the variation of positive and negative sequence components of voltages against the unbalance voltage factor UVF. The negative sequence voltage varies experimentally from 0 to 7.6% and 26.8% at open phase conditions, while the calculated results change from 21.59% to 34.87% in the case of the open phase. In addition, the positive sequence voltage varies experimentally from 100% to 103.65% and from 97.722% to 98.42% in the case of the open phase for the calculated results. Figure16 shows the effect of negative-sequence voltage on the negative sequence current generated by SERG. The resulting negative sequence current varies with the degree of unbalanced voltage factor linearly from 0 % to 31.735% for experimental results and from -19.9% to 36% for calculated results.
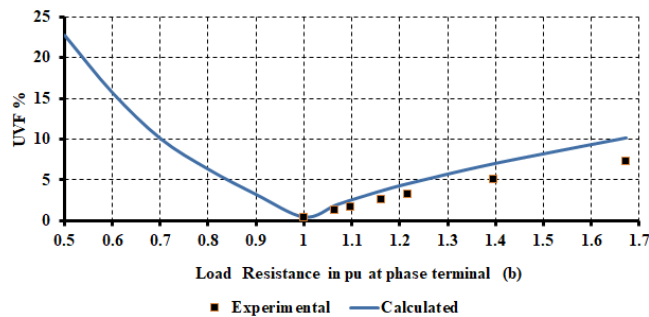

Figure 14. The UVF variation against unsymmetrical resistive load (pu) at phase (b)
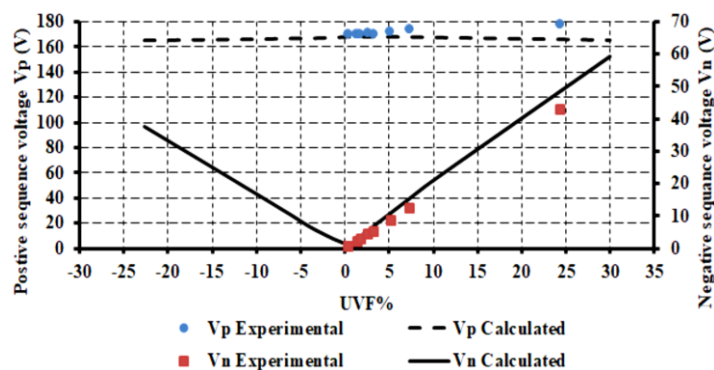

Figure 15. Variation of positive and negative sequence components of phase voltage against UVF at unsymmetrical load
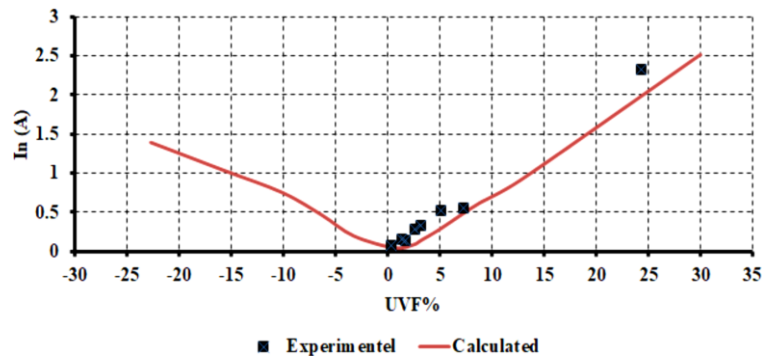
Figure 16. Variation of current negative sequence component against UVF at unsymmetrical load

4. CONCLUSION

This paper modeled and analyzed the stand-alone SERG under balanced and unbalanced operations. The mathematical analysis of symmetrical components is derived and studied in detail. The calculated results validated the proposed model and verified with experimental results of the laboratory SERG driven by a DC motor. In addition, the performance analysis of the generator is presented and analyzed under normal and unbalanced operations. The unsymmetrical loads and unsymmetrical excitation capacitances cases are studied and validated to represent the performance of SERG at unbalanced operation. The voltage and current sequence components are calculated by the symmetrical components method. The effects of both positive and negative sequence components on the UVF machine voltages, currents, electric torque, and electric power are studied.

REFERENCES

[1]   K. Wei, Y. Yang, H. Zuo, and D. Zhong, "A review on ice detection technology and ice elimination technology for wind turbine," *Wind Energy*, vol. 23, no. 3, pp. 433–457, Mar. 01, 2020. doi: 10.1002/we.2427.
[2]   T. R. Ayodele, A. S. O. Ogunjuyigbe, and B. B. Adetokun, "Optimal capacitance selection for a wind-driven self-excited reluctance generator under varying wind speed and load conditions," *Appl Energy*, vol. 190, pp. 339–353, 2017, doi: 10.1016/j.apenergy.2016.12.137.
[3]   D. Hammoumi, C. El Bekkali, M. Karim, M. Taoussi, N. El Ouanjli, and B. Bossoufi, "Direct controls for wind turbine with PMSG used on the real wind profile of essaouira-Morocco City," *Indonesian Journal of Electrical Engineering and Computer Science*, vol. 16, no. 3, pp. 1229–1239, Dec. 2019, doi: 10.11591/ijeecs.v16.i3.pp1229-1239.
[4]   Z. Alnasir, and M. Kazerani, "A small-scale standalone wind energy conversion system featuring SCIG, CSI and a novel storage integration scheme," *Renew Energy*, vol. 89, pp. 360–370, Apr. 2016, doi: 10.1016/j.renene.2015.12.041.
[5]   A. E. Hoffer, R. H. Moncada, B. J. Pavez, J. A. Tapia, and L. Laurila, "A high efficiency control strategy for synchronous reluctance generator including saturation," *2016 XXII International Conference on Electrical Machines (ICEM)*, 2016, pp. 39-45, doi: 10.1109/ICELMACH.2016.7732503.
[6]   H. H. H. Mousa, A. R. Youssef, and E. E. M. Mohamed, "Variable step size P&O MPPT algorithm for optimal power extraction of multi-phase PMSG based wind generation system," *International Journal of Electrical Power and Energy Systems*, vol. 108, pp. 218–231, Jun. 2019, doi: 10.1016/j.ijepes.2018.12.044.
[7]   N. K. S. Naidu, and B. Singh, "Experimental implementation of doubly fed induction generator-based standalone wind energy conversion system," *IEEE Trans Ind Appl*, vol. 52, no. 4, pp. 3332–3339, Jul. 2016, doi: 10.1109/TIA.2016.2542783.
[8]   T. Taluo, L. Ristić, and M. Jovanović, "Performance analysis of brushless doubly fed reluctance machines," *2019 20th International Symposium on Power Electronics (Ee)*, 2019, pp. 1-6, doi: 10.1109/PEE.2019.8923437.
[9]   T. R. Ayodele, and A. S. O. Ogunjuyigbe, "Wind energy resource, wind energy conversion system modelling and integration: a survey," *International Journal of Sustainable Energy*, vol. 34, no. 10, pp. 657–671, Nov. 2015, doi: 10.1080/14786451.2013.855778.
[10]   M. M. Ali, S. M. Allam, and T. H. Abdel-Moneim, "Dynamic characteristics of an isolated self-excited synchronous reluctance generator driven by a wind turbine," *Turkish Journal of Electrical Engineering and Computer Sciences*, vol. 24, no. 6, pp. 5238–5250, 2016, doi: 10.3906/elk-1412-6.
[11]   Y. H. A. Rahim, J. E. Fletcher, and N. E. A. M. Hassanain, "Performance analysis of salient-pole self-excited reluctance generators using a simplified model," *IET Renewable Power Generation*, vol. 4, no. 3, pp. 253–260, 2010, doi: 10.1049/iet-rpg.2009.0075.
[12]   A. S. O. Ogunjuyigbe, T. R. Ayodele, and B. B. Adetokun, "Steady state analysis of wind-driven self-excited reluctance generator for isolated applications," *Renew Energy*, vol. 114, pp. 984–1004, 2017, doi: 10.1016/j.renene.2017.07.110.
[13]   S. S. Maroufian, and P. Pillay, "Self-excitation criteria of the synchronous reluctance generator in stand-alone mode of operation," in *IEEE Transactions on Industry Applications*, Mar. 2018, vol. 54, no. 2, pp. 1245–1253, doi: 10.1109/TIA.2017.2764847.
[14]   M. Deepu Vijay, B. Singh, and G. Bhuvaneswari, "Standalone and grid-connected operations of a SynRG based WECS with BESS," *2018 IEEMA Engineer Infinite Conference (eTechNxT)*, 2018, pp. 1-6, doi: 10.1109/ETECHNXT.2018.8385286.
[15]   M. N. Ibrahim, E. M. Rashad, and P. Sergeant, "Steady-state analysis and stability of synchronous reluctance motors considering saturation effects," *2015 IEEE 10th International Symposium on Diagnostics for Electrical Machines, Power Electronics and Drives (SDEMPED)*, 2015, pp. 345-350, doi: 10.1109/DEMPED.2015.7303713.

[16] Y. Wang, and N. Bianchi, "Modeling and investigation of self-excited reluctance generators for wind applications," in *IEEE Transactions on Industry Applications*, vol. 55, no. 6, pp. 5809–5817, Nov.-Dec. 2019, doi: 10.1109/TIA.2019.2935931.

[17] J. S. Sedky, H. M. Yassin, H. H. Hanafy, and F. Ismail, "Voltage and frequency control of standalone wind-driven self-excited reluctance generator using switching capacitors," *Journal of Electrical Systems and Information Technology*, vol. 8, no. 1, Dec. 2021, doi: 10.1186/s43067-021-00030-1.

[18] F. Rebahi, A. Bentounsi, H. Khelifa, O. Boulkhrachef, and D. Meherhera, "Comparative study of a self-excited induction and synchronous reluctance generators capabilities," *2019 International Conference on Advanced Electrical Engineering (ICAEE)*, 2019, pp. 1-5, doi: 10.1109/ICAEE47123.2019.9014767.

[19] Y.-S. Wang, and L. Wang, "Steady-state performance of a self-excited reluctance generator under unbalanced excitation capacitors," *2000 IEEE Power Engineering Society Winter Meeting. Conference Proceedings (Cat. No.00CH37077)*, 2000, vol. 1, pp. 281-285, doi: 10.1109/PESW.2000.849972.

[20] Y. Chaturvedi, "Effects of magnetization characteristics on the performance of self-excited induction generator under unbalanced operations," *International Journal of System Assurance Engineering and Management*, vol. 13, no. 1, pp. 375–384, Feb. 2022, doi: 10.1007/s13198-021-01281-x.

[21] V. P. Suppioni, A. P. Grilo, and J. C. Teixeira, "Control methodology for compensation of grid voltage unbalance using a series-converter scheme for the DFIG," *Electric Power Systems Research*, vol. 133, pp. 198–208, Apr. 2016, doi: 10.1016/j.epsr.2015.12.034.

[22] E. L. Geraldi, T. C. C. Fernandes, A. B. Piardi, A. P. Grilo, and R. A. Ramos, "Parameter estimation of a synchronous generator model under unbalanced operating conditions," *Electric Power Systems Research*, vol. 187, Oct. 2020, doi: 10.1016/j.epsr.2020.106487.

[23] E. Nasr-Azadani, C. Cañizares, D. Olivares, and K. Bhattacharya, "Stability analysis of unbalanced distribution systems with synchronous machine and DFIG based distributed generators," *IEEE Transactions on Smart Grid*, vol. 5, no. 5, pp. 2326–2338 September 2014, doi: 10.1109/TSG.2014.2321709.

[24] V. P. Suppioni, A. P. Grilo, and J. C. Teixeira, "Improving network voltage unbalance levels by controlling DFIG wind turbine using a dynamic voltage restorer," *International Journal of Electrical Power and Energy Systems*, vol. 96, pp. 185–193, Mar. 2018, doi: 10.1016/j.ijepes.2017.10.002.

[25] A. H. Al-Bahrani, "Analysis of self-excited induction generators under unbalanced conditions," *Electric Machines and Power Systems*, vol. 24, no. 2, pp. 117–129, Mar. 1996, doi: 10.1080/07313569608955662.

[26] A. Ebadi, M. Mirzaie, and S. A. Gholamian, "Torque analysis of three-phase induction motor under voltage unbalance using 2D FEM," *International Journal of Engineering Science and Technology*, vol. 3, pp. 871-876, Feb. 2011.

[27] S. Kadiman, A. Basuki, and D. Suwarti, "Virtual laboratory of unbalanced transient condition in synchronous generator," *Indonesian Journal of Electrical Engineering and Computer Science*, vol. 5, no. 1, pp. 1–10, 2017, doi: 10.11591/ijeecs.v5.i1.pp1-10.

[28] E. Rezaei, M. Ebrahimi, and A. Tabesh, "Control of DFIG wind power generators in unbalanced microgrids based on instantaneous power theory," *IEEE Trans Smart Grid*, vol. 8, no. 5, pp. 2278–2286, Sep. 2017, doi: 10.1109/TSG.2016.2521644.

BIOGRAPHIES OF AUTHORS

Mostafa Rida ⓘ 🔍 SC ◖ was born in Cairo, Egypt on May 19, 1984. He received his BSc degree from Faculty of Engineering, Helwan University, Egypt in 2008. He received his M.Sc. degree in Electrical Power and Machines Engineering from Helwan University in 2015. Since 2016, he is working as an assistant lecturer at the Department of Electrical Engineering, Faculty of Engineering, Helwan University, Egypt. He is currently working towards the PhD at Helwan University, Egypt. His research interests are in Electrical Machines, Electrical Drives, Automation systems and Renewable Energy Systems. He can be contacted at email: Mostafarida@h-eng.helwan.edu.eg.

Essam Rashad ⓘ 🔍 SC ◖ was born in Shebin El-Kom, Egypt, in 1960. He received his BSc degree from the Department of Electric Power and Machines Engineering, Faculty of Engineering, Menoufiya University, Egypt in 1983. In 1987 and 1992 he received M.Sc. and PhD, respectively both from Faculty of Engineering, Alexandria University, Egypt. From 1985 to 1990, he was an offshore electrical engineer in Belayim Petroleum Company, Egypt. In 1992, he has joined Faculty of Engineering, Tanta University, Egypt, where he is currently a Full Professor since 2006. From Feb. to Aug 2000, he was a visiting researcher at the Faculty of Engineering, Nagasaki University, Japan. In the summer 2003, he was a visiting researcher at the Faculty of Engineering and Applied Science, Memorial University of Newfoundland, St. John's, Canada. From 2004 to 2009, he was Head of Electrical Technology Department, Buraydah College of Technology, Kingdom of Saudi Arabia. From 2011 to 2014, he was Vice Dean for Education and Student Affairs of Faculty of Engineering, Tanta University, Egypt. He was Head of Electrical Power and Machines Engineering from 2009 to 2011 and from 2014 to September 2020. He was the General Chairman of the 21st International Middle East Power Systems Conference (MEPCON'2019), Cairo, December 2019 and a Co-Chairman of the First IEEE Conference on Power Electronics and Renewable Energy, Aswan-Egypt, October 2019. Prof. Rashad is an IEEE senior member since 2002. In 2019, he obtained the Outstanding Engineering Award for "Outstanding Contribution in the Electrical Power Engineering Education, Research and Industry" from IEEE-PES (Power and

Energy Society), Egypt Chapter. Prof. Rashad has published more than 160 technical conference and journal papers. His research interests include electrical machine analysis and design, electrical drives, power electronics, micro-grids, distributed generation, and renewable energy systems. He can be contacted at email: emrashad@ieee.org.

Adel El-Samahy ⓘ 🔍 SC ◖ was born in Egypt, on September 5, 1958. He received the B.Sc. degree in Electrical Engineering in 1981 from Faculty of Engineering, Alexandria University, Alexandria, Egypt. He received M.Sc. and Ph. D. in Electrical engineering from University of Helwan, Cairo, Egypt on 1988 and 1993. He served as a visiting scholar and researcher at University of Washington, Seattle, USA, from 1990 to 1992. Currently, he is a professor in electrical power and machines Engineering department at the Faculty of Engineering, Helwan University. Professor Adel El-Samahy has a strong academic background in the field of renewable energy systems, power electronics, electrical machines, electric drives, advanced control, and artificial intelligence. He is currently involved in four international funded projects. These projects include EUROSUNMED- Europe Mediterranean Cooperation on Research & Training in Sun Based Renewable Energies, EC-FP7, 6.3 M Euro, 22M Euro FP7 fund, STS-MED- Small scale thermal district units for Mediterranean communities, 5 M Euro, EU-ENPI program, Multipurpose Applications by Thermo-dynamic Solar project (MATS) , 22M Euro FP7-ENERGY-2010, 22M Euro, and EAC/a03/2016 High level High level rEnewaBle and energy efficency mAster courses/HEBA rEnewaBle and energy efficency mAster courses / HEBA. He is the author of more than 40 scientific research articles published in leading international journals and international conferences. He is also a reviewer for multiple international journals. He can be contacted at email: a.elsamahy@h-eng.helwan.edu.eg.

Mohamed EL-korfolly ⓘ 🔍 SC ◖ was born in Egypt, on January 23, 1946. He received the B.Sc. degree in Electrical Engineering in 1969 from Faculty of Engineering and Technology, Helwan University, Egypt. He received M. Sc.in 1981 from Faculty of Engineering and Technology, Helwan University, Egypt and Ph.D. in 1986 fromUMIST, The Victoria University of Manchester, England. Currently, he is an associate professor in electrical power and machines Engineering department at the Faculty of Engineering, Helwan University. Associate Professor Mohamed elkorfolly has a strong academic background in the field of power electronics, electrical machines, electric drives, advanced drives and renewable energy systems. He was cooperating in Improvement of Starting Performance of Large synchronous Motor Drive, FRCU, No. MS/89014, 1991 and teaching training courses in Power electronics for Petroleum Companies Tech. Training Center, Egypt, Tourah Cement Company, Egypt, and El Masria Cement Company, Egypt, training courses of Static and Digital Protective relaying for Engineers of Iron and Steel Company, Egypt and training courses of Speed Control Of Electric Motors in Aluminum Naga Hamady, Egypt. He is the author of more than 20 scientific research articles published in leading international journals and international conferences. He can be contacted at email: mohamed_elkorfoly@h-eng.helwan.edu.eg.

Erhab Youssef ⓘ 🔍 SC ◖ received B.S. and M.S. degree in electrical power and machines engineering from Helwan University, Cairo, Egypt in 2005 and 2012 respectively. Since 2007, She was assistant lecturer in Electrical Power and Machines department, Helwan university. In 2017, she obtained a scholarship to complete her Ph.D in Instituto Superior Técnico, University of Lisbon, Portugal. In 2020, she awarded a dual Ph.D. degree from Lisbon University and Helwan University. Currently, she is working in Helwan University as Assistant Professor in Electrical Power department. Her research interest includes integration of renewable energy into grid, FACTS, power converters, power system stability and microgrid. She can be contacted at email: erhabyoussef@h-eng.helwan.edu.eg.